Engineering 2015, 1(3): 344–350
DOI 10.15302/J-ENG-2015077

Research
Medical Instrumentation—Article

Characterizing Thermal Augmentation of Convection-Enhanced Drug Delivery with the Fiberoptic Microneedle Device

R. Lyle Hood[1], Rudy T. Andriani[2], Tobias E. Ecker[2], John L. Robertson[3], Christopher G. Rylander[4*]

ABSTRACT Convection-enhanced delivery (CED) is a promising technique leveraging pressure-driven flow to increase penetration of infused drugs into interstitial spaces. We have developed a fiberoptic microneedle device for inducing local sub-lethal hyperthermia to further improve CED drug distribution volumes, and this study seeks to quantitatively characterize this approach in agarose tissue phantoms. Infusions of dye were conducted in 0.6% (w/w) agarose tissue phantoms with isothermal conditions at 15 °C, 20 °C, 25 °C, and 30 °C. Infusion metrics were quantified using a custom shadowgraphy setup and image-processing algorithm. These data were used to build an empirical predictive temporal model of distribution volume as a function of phantom temperature. A second set of proof-of-concept experiments was conducted to evaluate a novel fiberoptic device capable of generating local photothermal heating during fluid infusion. The isothermal infusions showed a positive correlation between temperature and distribution volume, with the volume at 30 °C showing a 7-fold increase at 100 min over the 15 °C isothermal case. Infusions during photothermal heating (1064 nm at 500 mW) showed a similar effect with a 3.5-fold increase at 4 h over the control (0 mW). These results and analyses serve to provide insight into and characterization of heat-mediated enhancement of volumetric dispersal.

KEYWORDS near-infrared laser, thermochemotherapy, agarose, photothermal heating, micro-catheter, malignant glioma

1 Background and objectives

Many novel approaches have been developed to circumvent the blood-brain barrier and deliver pharmaceuticals to intracerebral targets [1–5]. Convection-enhanced delivery (CED) is a promising technique that avoids this issue through using catheters to infuse drugs locally within intracerebral targets [6–8]. To accomplish this, one or more catheters are inserted through a burr-hole in the skull and advanced to a target site. Once placed, a gradual, continuous infusion is maintained to provide pressure-driven flow for the infusate of interest. CED approaches have been developed for treating neurodegenerative, epileptiform, and neoplastic maladies [7, 9–13]. Due to pressure limitations on feasible infusion rates, CED is frequently maintained at a slow rate for up to several days. Often compared to biodegradable polymer delivery systems, CED has been demonstrated to increase effective tissue penetration of infused drugs by over an order of magnitude relative to diffusion-based methods without causing cerebral edema [14, 15]. The method is particularly attractive for delivering larger molecules that cannot bypass the blood-brain barrier and have lower effective rates of diffusion, such as antibodies, chemotherapeutics, and immunotoxins [16–21]. Unfortunately, the PRECISE study, the first multi-center trial utilizing CED to treat malignant glioma, did not meet required minimum clinical outcomes. In a retrospective analysis by Sampson et al., this failure was attributed to CED not achieving sufficient dissemination of the chemotherapeutic immunotoxin throughout malignant volumes and the surrounding margins [22]. Despite these discouraging results, many groups still seek better strategies and solutions to leverage CED into a viable clinical tool.

Another strategy for enhancing the penetration of infused chemotherapeutic agents is thermochemotherapy, as heating of the drug solution has been shown to substantially increase the effective depth of treatment [23]. In addition, adjunctive hyperthermia has been demonstrated to significantly increase the cytotoxic capacity of many chemotherapeutic agents [24–26]. DeWitt et al. demonstrated that mild hyper-

[1] Department of Nanomedicine, Houston Methodist Research Institute, Houston, TX 77030, USA; [2] Department of Mechanical Engineering, Virginia Tech, Blacksburg, VA 24060, USA; [3] School of Biomedical Engineering, Virginia Tech, Blacksburg, VA 24060, USA; [4] Department of Mechanical Engineering, University of Texas, Austin, TX 78712, USA
* Correspondence author. E-mail: cgr@austin.utexas.edu
Received 1 August 2015; received in revised form 21 August 2015; accepted 4 September 2015

thermia could also increase the drug uptake into the cell, which was attributed to plasma membrane permeabilization [27]. This group has developed a technological solution enabling a combination of thermochemotherapy with intracranial CED via a novel fiberoptic catheter, the fiberoptic microneedle device (FMD), which enables co-delivery of fluid agents and laser energy. This design and its fabrication methods have been described previously [28], as have characterizations of its mechanical penetration, light-guidance, and fluid delivery [28–31]. This group previously demonstrated that photothermal heating at the point of infusion could increase volumetric dispersal of contrast agents delivered through CED within an *in vivo* rodent model [28].

This study sought to determine if the volumetric dispersal enhancement seen in rodent models was also observed in agarose phantoms and, if so, to begin characterizing the heat-mediated dispersal increase. Agarose tissue phantoms at a weight ratio of 0.6% are an accepted simulacrum of cerebral tissue [32, 33] and allow direct observation of infused volumes. Initial experiments mimicked our previous *in vivo* approaches through delivering contrast agents into agarose with concurrent photothermal heating. To better quantify thermal effects, additional experiments characterized infusions into agarose volumes heated at near-isothermal conditions via waterbath, removing the anisotropic photothermal heating element. These experiments utilized a simplified catheter prototype using a non-light-guiding silica capillary of identical dimensions to our co-delivery FMD design (365 μm in outer diameter (OD); 150 μm in inner diameter (ID)). Further analysis focused on characterizing the heat-mediated changes to dispersal of infused contrast agents.

2 Materials and methods

2.1 Fiberoptic microneedle device designs

To determine if agarose exhibited a heat-mediated increase in volumetric disposal, an experiment was conducted with a two-fiber FMD design. FMD catheters were created through bonding fused silica capillary tubing (150 μm/365 μm ID/OD, Polymicro Technologies, Phoenix, AZ, USA) along the length of a multimode fiberoptic (100 μm/110 μm/125 μm core/cladding/buffer, numerical aperture (NA) = 0.22, Polymicro Technologies, Phoenix, AZ, USA). A nested syringe-needle system was necessary to allow fluid coupling into the capillary without running the fiberoptic through the fluid line. One end of the capillary was epoxied into the tip of a 22G dispensing needle, while the infusing length extended ~ 10 cm beyond the needle. This setup enabled fluid coupling via the dispensing needle's Luer-Lock. The capillary and 22G needles were threaded alongside the fiberoptic into a secondary 18G needle that acted as a housing. The endfaces of the fiberoptic and capillary co-terminated 2.5 cm from the tip of the 18G housing. Following immobilization of the glass fibers, the housing was filled with epoxy to promote lateral stability. This assembly is depicted in Figure 1.

A simplified FMD prototype was employed for isothermal agarose infusions with the goal of simplifying the heating profile to better characterize the heat-mediated transport. These

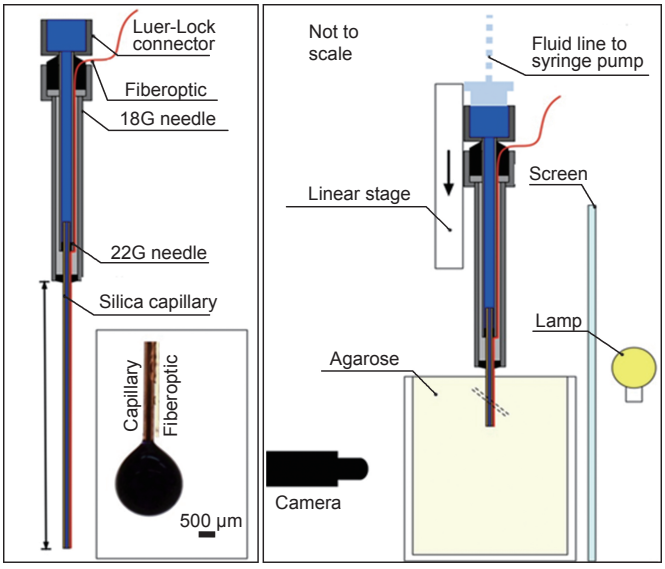

Figure 1. (a) Depiction of FMD design; (b) experimental setup.

FMDs were fabricated through adhering fused silica capillary tubing within a 1 in (1 in = 2.54 cm), 22G, stainless-steel dispensing needle (McMaster-Carr, Atlanta, GA, USA). The capillary tubing was cut to 3.75 cm in length and adhered within the dispensing needle so that the capillary extended 2.5 cm from the blunt end of the dispensing needle. This assembly is shown in Figure 2. The Luer-Lock fluid couple at the proximal end of the dispensing needle allowed attachment to the fluid system.

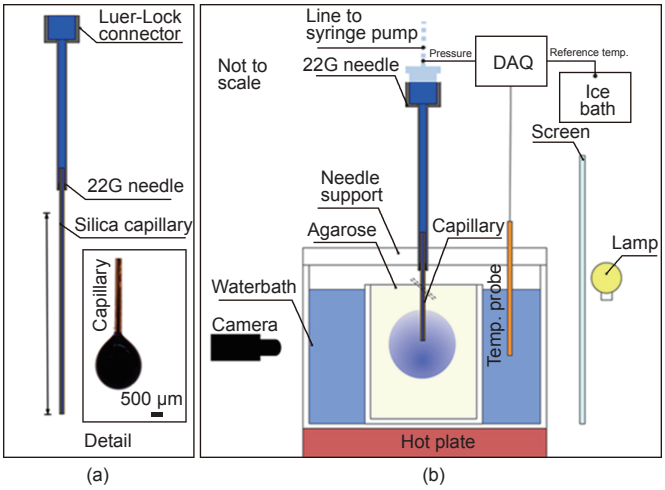

Figure 2. (a) The FMD assembly made from a 22G needle and a length of silica capillary, with an inset showing the tip; (b) a diagram of the experimental setup: The diagram is simplified to a single needle, although actual experiments were done with three needles in parallel (into the page from this perspective) delivering simultaneously. DAQ stands for data acquisition unit.

2.2 Co-delivery into agarose

The proof-of-concept co-delivery infusions with the two-fiber FMDs were conducted within rectangular, polystyrene molds (1.7 cm × 8.1 cm × 3.9 cm) open at the top. An agarose (certified molecular biology grade, Bio-Rad Laboratories, Hercules, CA, USA) solution was mixed at 0.6% (w/w) with de-ionized water, boiled, and decanted into the molds after a brief cool-

ing period. The molds were wrapped in paraffin wax and refrigerated at 4 °C overnight prior to use. For the experiment, the agarose was removed from refrigeration and allowed to return to room temperature. Appropriate warming was established through measurement with a T-type thermocouple and a HH127 Data Logger (Omega Engineering, Stamford, CT, USA).

A custom shadowgraphy framework was used as previously described [34]. Briefly, a light-diffusing acrylic sheet was mounted in an aluminum window. An attached micrometer (OptoSigma, Santa Ana, CA, USA) allowed the precision-controlled insertion of FMD catheters. The framework enabled backlit visualization of the infused volume and vertical, guided insertion of the two-fiber FMD into the agarose volumes. A schematic of this setup is shown in Figure 1. Infusions into agarose were conducted at a flow rate of 1 $\mu L \cdot min^{-1}$. Laser irradiation was provided by a 1064 nm CW diode-pumped fiber laser (IPG Photonics, Oxford, MA, USA). A laser power of 500 mW was determined to heat the agarose volume to a steady-state increase in temperature of 4–5 °C within a two-hour period in preliminary experiments (data not shown). A free space-to-fiberoptic coupler (Newport Corporation, Irvine, CA, USA) was utilized for coupling light into the FMD's multimode fiberoptic. The coupling efficiency was established prior to every insertion with an integrating sphere (Newport Corporation, Irvine, CA, USA). The capillary tube was connected via a micro-IV extension set to a 10 mL syringe (containing 5% FD&C Blue #2) actuated by a PHD Ultra syringe pump (Harvard Apparatus, Holliston, MA, USA).

The FMD was rapidly inserted into the agarose manually, guided by the micrometer's rails. Rapid catheter insertion has been demonstrated to reduce backflow by quickly overcoming the viscoelastic compression of the media [35]. Following manual insertion approximately 1.25 cm within the agarose, the micrometer was used to precisely place the tip 1.5 cm from the surface. Finally, the catheter tip was raised by 1 mm, which was shown by Martanto et al. to aid in removing any coring of the agarose into the capillary [36].

Following successful insertion, fluid infusion at 1 $\mu L \cdot min^{-1}$ and laser irradiation at a delivery of 500 mW were begun simultaneously. Photographs were automatically captured once per minute from an angle perpendicular to the catheter's body through the transparent polystyrene mold and agarose. An OPP-M fiberoptic sensor (OpSens Inc., Québec City, Québec, Canada) monitored the line pressure at the syringe pump. If line pressure reached 40 mmHg (1 mmHg ≈ 1.33×10^2 Pa), the system was considered clogged and the tip was raised and lowered 1 mm by the micrometer to alleviate any coring within the catheter's tip. Infusion was ceased and all data discarded if line pressure reached 60 mmHg or dye dispersal contacted the polystyrene mold surface.

2.3 Isothermal agarose infusions

A custom infusion setup was designed for conducting agarose infusions in waterbaths to provide a repeatable, near-isothermal environment. T75 flasks (Corning Inc., Corning, NY, USA) were modified by drilling four ports into the narrow side of the container: three for FMD insertion and one for a micro-thermocouple (Omega Engineering, Stamford, CT, USA). To better isolate thermal effects from disturbance of the agarose during insertion, the FMDs were cast within the agarose. Three FMDs were pressed firmly into the drilled ports of each flask and epoxied into place. Each FMD had a polyimide-jacketed fused-silica fiber (125 μm in OD) inserted through its hollow bore to exclude liquid agarose rising into the tube through capillarity during the cure process. A plug of removable hot glue was used to temporarily seal the thermocouple port. Three-way T-couples were attached to the Luer-Lock connector of each 22G needle. The fiberoptics passed through the T-couple and extended beyond the top. This assembly provided a submersible housing for the agarose volume. The agarose was prepared and decanted into T75 flasks as described above. The flasks were capped and placed on their sides (T-couples facing upwards) in 4 °C refrigeration for at least 24 h prior to use. A small amount of de-ionized water was injected through each T-couple and left within the T-couple/FMD to exclude air during the cure process.

Once the agarose had set, the flasks were removed from refrigeration. The fused silica fibers were carefully removed from the FMDs. Syringes (3 mL in BD) secured within a syringe pump (Harvard Apparatus, Holliston, MA, USA) were coupled individually to each T-couple on the flask via micro-IV extension (Smiths Medical ASD, Inc., Dublin, OH, USA) lines. Both the syringes and extension sets were filled with 5% (w/w) FD&C Blue #2 dye prior to connection with the FMDs. The dye was allowed to diffuse freely throughout the de-ionized water within the T-couple, which did not dilute the dye sufficiently to interfere with the shadowgraphic measurements. The hot glue over the thermocouple port was carefully removed and a T-type micro-thermocouple was inserted into the agarose. A large, transparent, plastic vessel served to contain the waterbath. The agarose-filled T75 flask and connected fluid lines were gently placed into the bath. The bath temperature was regulated by a water heater/chiller (ThermoNeslab RTE 7 Chiller, Newington, NH, USA). Near-isothermal environments were maintained at four different experimental temperatures: 15 °C, 20 °C, 25 °C, and 30 °C. T-type thermocouples were placed within the free fluid of the waterbath and an exterior beaker of ice water, which served as a cold junction for calibration. All T-type thermocouple measurements were recorded on a HH127 Data Logger (Omega Engineering Inc., Stamford, CT, USA).

Once the target isothermal environment was achieved, the syringe pump was activated to provide an infusion rate of 1 $\mu L \cdot min^{-1}$ for 100 min. Temperatures within the agarose were maintained within ± 2 °C of their target or the infusion set was discarded. Line pressure for each infusion was monitored with wet/wet differential pressure sensors (Omega Engineering Inc., Stamford, CT, USA) connected in parallel with the micro-IV extension lines via the T-couples. The sensors were controlled by an eight-channel data-acquisition unit (Omega Engineering Inc., Stamford, CT, USA) connected to a

laptop. A schematic of the experimental setup is provided in Figure 2. The experimental setup was backlit with a bright lamp, allowing contrast shadowgraphy measurements to be taken through photographing the contralateral side of the agarose volume. Photographs were automatically captured once per minute by a Canon EOS Rebel T1i/EOS 500D camera (Canon USA, Lake Success, NY, USA).

2.4 Poroelastic model

A model developed by Chen et al. was modified and fit to the data in order to capture the temperature dependent effect on volumetric dispersal rate [37]. Their study focused on modeling volumetric distribution as a function of infusion rate, whereas the isothermal experiments in this study sought to determine volumetric distribution as a function of temperature. Beginning with volume continuity and a modified Darcy's law describing the poroelastic case, Chen et al. developed a description of volume of distribution (V_d) as a function of pore fraction (φ), dilatation (e), and time (t). The deformation behavior of the agarose's porous frame was captured by modifying the equations that describe convective transport through rigid porous media. The dilatational diffusion constant (D_d) is defined as, which includes contributions from the Darcy permeability of the agarose (k) as well as the material rigidity (λ) and compressibility (μ), moduli. If steady-state (where $t >> r^2/D_d$) is assumed, the transient contributions of the agarose's rigidity and compressibility can be ignored. This allows the pore fraction to be written as a function of radius:

$$\varphi(r,t) \approx \frac{A+\varphi_0 r}{A+r} \tag{1}$$

where A is defined as $A = q/(4\pi D_d)$, in which q is the volumetric flow rate; φ_0 is the initial pore fraction ($t = 0$); r is the radius. If the volume, after a very long time frame, is equal to the total infused volume ($V_{inf} = qt$), the radius R of the resulting volume of distribution within the agarose can be calculated by the equation:

$$V_{inf} = \int_{r_0}^{R} dr \cdot 4\pi r^2 \varphi(r,t) \tag{2}$$

As agarose is a viscoelastic medium, its material properties vary with temperature. These contributions are captured within the D_d parameter, although decoupling the influences of Darcy permeability and the material moduli was not possible with this experimental approach. In this experiment, we were able to directly calculate V_d as a function of time and temperature. This was achieved through algorithmic post-processing of infusions over a series of time-sequence images. Following the precedent set by Chen et al. of analyzing volumetric dispersal at 100 min, we calculated $D_d(T)$ at 100 min through its relation to $V_d(T)$ and applied an exponential regression to describe the distribution:

$$D_d(T)\big|_{t=100\ \text{min}} = ae^{bT} \tag{3}$$

where a and b are constants equaling 5.739×10^{-8} and -0.05678, respectively. By applying this regression to Eq. (2), one can describe a relationship between $R(T)^3$ and $D_d(T)$, which allows direct prediction of $V_d(T)$ as

$$V_d(T) = \frac{4}{3}\pi R(T)^3 \tag{4}$$

This relation for D_d as a function of temperature provides a steady-state, empirical prediction of the temperature dependent volumetric dispersal that should be adaptable to other agarose models or even as a component of the distribution within living tissue.

3 Results

3.1 Co-delivery agarose infusions

Volumetric dispersal in the co-delivery infusion experiments was calculated once per minute through analysis of captured photographs. This group has previously demonstrated that this method has an associated error of less than 5% [34]. This data is shown in Figure 3(a). Each curve represents an average of $N = 5$ experiments. Exclusion criteria included dye-front contact with the agarose boundaries, temperature variation of > ± 2 °C of the target, and line pressure exceeding 60 mmHg. Co-delivery exhibited a substantially enhanced volumetric dispersal relative to infusion-only controls. Analysis of the distance of forward distribution from the catheter's tip for every frame is provided in Figure 3(b). Co-delivery was associated with significantly enhanced forward progress of the dye. However, as the photothermal heating was highly anisotropic and nontrivial to measure or estimate, experiments utilizing uniformly heated agarose volumes were conducted to better establish the relationship between temperature and volumetric dispersal.

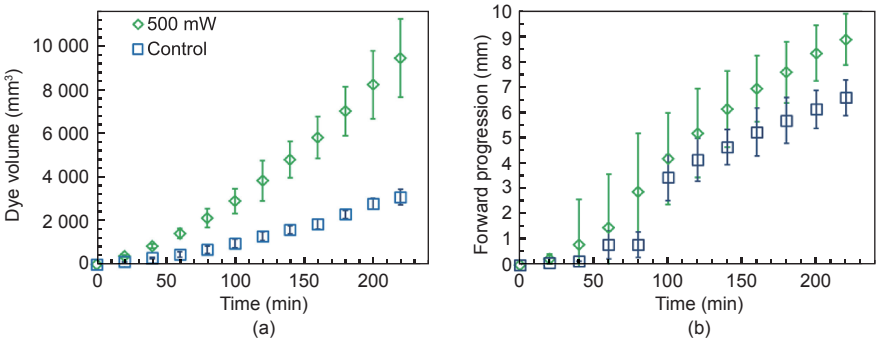

Figure 3. (a) Data from the co-delivery experiment exhibiting the volumetric dispersal; (b) the forward dye progression for the 500 mW irradiation and infusion-only groups. Error bars depict two standard deviations.

3.2 Isothermal agarose experiment results

At least $N = 4$ experiments for each temperature were included in the volume distribution analysis. Volumetric dispersal rate positively correlated with increasing temperature, and the 100 min average of V_d at 30 °C was over 7-fold greater than the 15 °C average at the same time point. Figure 4 provides a plot of the volume distribution as a function of time for each temperature as well as representative images

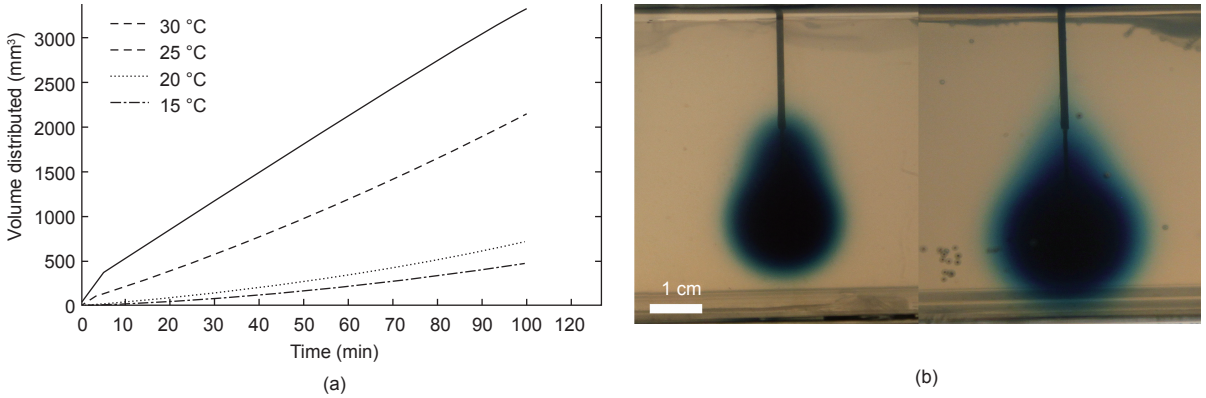

Figure 4. (a) Volume distributed versus time for each experimental temperature; (b) representative images of isothermal infusions at 15 °C (left) and 30 °C (right) after 100 min.

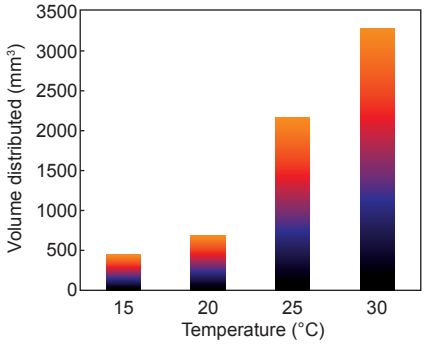

Figure 5. Plot showing volume distributed at 100 min for each temperature data set. Error bars depict the calculated standard error.

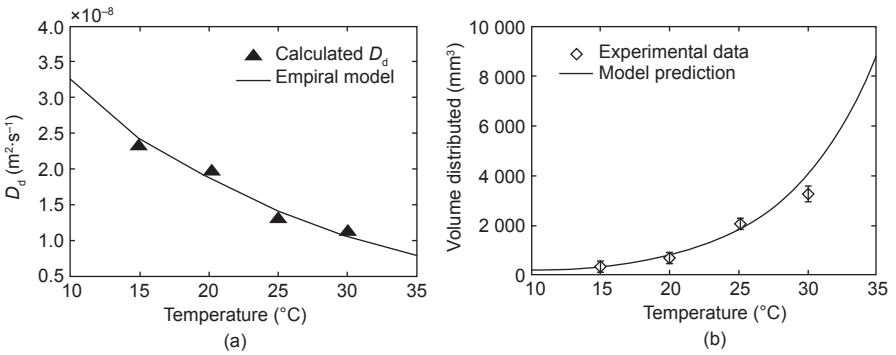

Figure 6. (a) Calculated dilatational diffusion coefficients for each temperature with an exponential regression; (b) measured volume distribution values as a function of temperature at 100 minutes plotted with the empirical model prediction.

from the 15 °C and 30 °C experiments at 100 min.

Line pressure averaged (29.1 ± 11.0) mmHg, (29.3 ± 6.8) mmHg, (20.5 ± 1.0) mmHg, and (29.7 ± 5.6) mmHg for the 15 °C, 20 °C, 25 °C, and 30 °C sets, respectively. These results suggested that volumetric flow rate had no dependence on line pressure; although it should be noted that line pressure may not be indicative of pressure within the diffusing dye volume. To determine statistical significance and provide a time point for the theoretical analysis described below, the volume at 100 min was chosen as a comparison point between the different populations. Figure 5 shows a bar plot of the distributed volume for each temperature at 100 min. A student *t*-test showed each of the populations to be statistically different at $P < 0.05$. The lack of correlation between standard deviations shown for each group and for respective line pressures provides further evidence of the independence of volumetric dispersal from line pressure.

3.3 Model development

Chen et al. estimated values for the different constants by employing a simultaneous least-squares procedure on a cost-function involving their measured and predicted pressure and distribution volume data [38]. This group used the empirically derived constants from Chen et al. and experimentally measured V_d values to describe the dilatation diffusion constant D_d at each agarose temperature. An exponential regression was determined to provide the best fit at most volumetric dispersal time points through R^2 value comparison between quadratic, exponential, and power law regressions in MATLAB. This regression enabled a theoretical prediction for volume distribution as a function of temperature. Figure 6 shows a plot of the experimental data after 100 min of infusion and the theoretical prediction.

4 Discussion

The isothermal experiments sought to quantify the relationship between the rate of volume increase and the temperature of the agarose. Experiments at 15 °C, 20 °C, 25 °C, and 30 °C demonstrated a positive correlation between increased temperature and volumetric dispersal. Analysis of these data showed that the 30 °C average at 100 min was over seven times greater than the 15 °C average at the same time point. The empirical predictive model described an exponential increase in the volumetric dispersal rate; an intuitive result, as increasing radial transport orthogonal to the point of infusion would cause a cubic rise in infusion volume. As the same fluid volume is being infused between each isothermal temperature, suggesting that the infusion volume has a lower concentration at higher temperatures as well. This implication is an important factor to note if this approach is to be applied to slow infusion treatments such as CED.

This group has previously demonstrated enhanced volumetric dispersal of infused contrast agents through concurrent photothermal heating [28]. The work described in this paper is the first step to developing a comprehensive predictive model of the *in vivo* case. The homogeneous agarose model enabled empirical predictions through symmetry-based simplification of a one-dimensional system. While these results are limited to the idealized isothermal case, the dispersal rate determined for each temperature provides a foundation for modeling the asymmetric, spatially variable temperatures generated by photothermal heating. As intracerebral treatments are expensive and relatively high risk, accurate pre-intervention simulations should enable clinicians to better adapt their approach to specific patients and indications.

Analysis of the co-delivery infusions correlated well with the idealized isothermal case. Quantifying the infusion volume's forward advancement along the beam path exhibited an expected increase of the dispersal rate. The infusion volume exhibited a greater forward distribution along the beam path, but analysis also indicated that forward progress increased orthogonally from the length of the catheter as well, but to a lesser degree. This result may be attributable to thermal conduction. Standard deviation increased over time for both groups, but more markedly for the co-delivery infusions. This finding is potentially attributable to small differences in local dye concentration caused by the manual insertion method, resulting in variation in heat distribution throughout the diffusing volume. In an *in vivo* scenario, the high scattering coefficient of most tissues, including cerebral tissues, would much more rapidly reduce the directionality of the light and create a more spherical heating volume. However, the degree to which this effect influences heating will vary with tissue type and needs to be determined experimentally.

The isothermal experiment was purposefully designed to provide a more simplistic look at the heat-mediated volumetric dispersal increase in order to aid in decoupling the influences of temperature gradients. Ideally, the injected fluid has the same temperature as the agarose, and therefore no temperature gradient exists and no natural convection takes place. Considering the relatively low injection volume flow rate and the fact that the fluid lines are inserted into the bath as well, we can assume that natural convection due to density differences of the fluid in the agarose compound and the injected fluid is minimized. In the case of the co-delivery infusion, this effect is more complex. Firstly, the localized heating changes the permeability, which has a direct influence on the convection through the porous media. Secondly, the localized heating may change the fluid density, which influences the flow due to buoyancy—especially where the forced convection is weak. This factor would cause the fluid in the beam path to rise toward the needle tip. The fact that we still see improved forward distribution indicates that the forced convection counteracts the free convection for the cases studied.

There are many limitations in an agarose phantom's simulation of living tissue. Agarose's lack of blood perfusion, isotropic composition, and lack of cellularity are substantially different from living tissue. However, 0.6% agarose was established by Chen et al. as a reasonable model for cerebral tissue, and has been frequently used in the literature [32, 39, 40]. This may represent a very conservative estimate of volumetric dispersal variance, as phenomena in living tissue, such as blood perfusion, would react synergistically with low-level hyperthermia to further increase dispersal of infused fluid. The agarose data provided here correlates well with a previous *in vivo* study published by this group wherein sub-lethal heating during infusion into rodent brains was shown to significantly increase dispersal [28]. The conservation of the heat-mediated effects on infusion dispersal volume further supports the use of 0.6% agarose as a tissue phantom capable of predicting certain *in vivo* phenomena.

5 Conclusions

This study demonstrated that photothermal heating would increase the distribution of infused contrast agents within agarose tissue phantoms. The temperature-mediated enhancement in volumetric dispersal rate was determined experimentally through shadowgraphy and image-processing techniques. Isothermal infusions were conducted at 15 °C, 20 °C, 25 °C, and 30°C. These infusions showed a positive correlation between temperature and V_d, with V_d at 30 °C showing a 7-fold increase at 100 min over the 15 °C isothermal case. Photothermal co-delivery at 500 mW into room-temperature agarose showed a very similar effect with a 3.5-fold increase at 4 h over the control (0 mW). These results motivate further exploration of the potential role of concurrent photothermal heating in enhancing the tissue penetration of chemotherapeutics and other therapeutic agents.

Acknowledgements

The authors would like to acknowledge the Coulter Foundation and NIH (NIH/NCI 1R21CA156078) for their funding of this project. Fiberoptic microneedle device fabrication methods and applications are described in US patent application 13/203800 and PCT/US2012/026968, which are managed by the Virginia Tech Intellectual Properties Group.

Compliance with ethics guidelines

R. Lyle Hood, Rudy T. Andriani, Tobias E. Ecker, John L. Robertson, and Christopher G. Rylander declare that they have no conflict of interest or financial conflicts to disclose.

References

1. C. V. Pardeshi, V. S. Belgamwar. Direct nose to brain drug delivery via integrated nerve pathways bypassing the blood-brain barrier: An excellent platform for brain targeting. *Expert Opin. Drug Deliv.*, 2013, 10(7): 957–972
2. B. S. Bleier, R. E. Kohman, R. E. Feldman, S. Ramanlal, X. Han. Permeabilization of the blood-brain barrier via mucosal engrafting: Implications for drug delivery to the brain. *PLoS One*, 2013, 8(4): e61694
3. M. Aryal, C. D. Arvanitis, P. M. Alexander, N. McDannold. Ultrasound-mediated blood-brain barrier disruption for targeted drug delivery in the

central nervous system. *Adv. Drug Deliv. Rev.*, 2014, 72: 94–109
4. F. Dilnawaz, A. Singh, S. Mewar, U. Sharma, N. R. Jagannathan, S. K. Sahoo. The transport of non-surfactant based paclitaxel loaded magnetic nanoparticles across the blood brain barrier in a rat model. *Biomaterials*, 2012, 33(10): 2936–2951
5. P. A. Garcia, et al. 7.0-T magnetic resonance imaging characterization of acute blood-brain-barrier disruption achieved with intracranial irreversible electroporation. *PLoS One*, 2012, 7(11): e50482
6. D. W. Laske, R. J. Youle, E. H. Oldfield. Tumor regression with regional distribution of the targeted toxin TF-CRM107 in patients with malignant brain tumors. *Nat. Med.*, 1997, 3(12): 1362–1368
7. R. H. Bobo, D. W. Laske, A. Akbasak, P. F. Morrison, R. L. Dedrick, E. H. Oldfield. Convection-enhanced delivery of macromolecules in the brain. *Proc. Natl. Acad. Sci. U.S.A.*, 1994, 91(6): 2076–2080
8. K. S. Bankiewicz, et al. Convection-enhanced delivery of AAV vector in parkinsonian monkeys; *in vivo* detection of gene expression and restoration of dopaminergic function using pro-drug approach. *Exp. Neurol.*, 2000, 164(1): 2–14
9. L. C. Vazquez, et al. Polymer-coated cannulas for the reduction of backflow during intraparenchymal infusions. *J. Mater. Sci. Mater. Med.*, 2012, 23(8): 2037–2046
10. S. S. Gill, et al. Direct brain infusion of glial cell line-derived neurotrophic factor in Parkinson disease. *Nat. Med.*, 2003, 9(5): 589–595
11. M. A. Rogawski. Convection-enhanced delivery in the treatment of epilepsy. *Neurotherapeutics*, 2009, 6(2): 344–351
12. J. H. Sampson, et al. Intracerebral infusate distribution by convection-enhanced delivery in humans with malignant gliomas: Descriptive effects of target anatomy and catheter positioning. *Neurosurgery*, 2007, 60(2 Suppl 1): ONS89-98; discussion ONS98-9
13. J. F. Hamilton, et al. Heparin coinfusion during convection-enhanced delivery (CED) increases the distribution of the glial-derived neurotrophic factor (GDNF) ligand family in rat striatum and enhances the pharmacological activity of neurturin. *Exp. Neurol.*, 2001, 168(1): 155–161
14. A. A. Kanner. Convection-enhanced delivery. In: G. H. Barnett, ed. *High-Grade Gliomas: Diagnosis and Treatment*. Totowa, NJ: Humana Press, 2007: 303–314
15. W. A. Vandergrift, S. J. Patel, J. S. Nicholas, A. K. Varma. Convection-enhanced delivery of immunotoxins and radioisotopes for treatment of malignant gliomas. *Neurosurg. Focus*, 2006, 20(4): E13
16. M. Bettag, et al. Stereotactic laser therapy in cerebral gliomas. *Acta Neurochir. Suppl. (Wien)*, 1991, 52: 81–83
17. A. Carpentier, et al. MR-guided laser-induced thermal therapy (LITT) for recurrent glioblastomas. *Lasers Surg. Med.*, 2012, 44(5): 361–368
18. H. J. Schwarzmaier, I. V. Yaroslavsky, A. N. Yaroslavsky, V. Fiedler, F. Ulrich, T. Kahn. Treatment planning for MRI-guided laser-induced interstitial thermotherapy of brain tumors—The role of blood perfusion. *J. Magn. Reson. Imaging*, 1998, 8(1): 121–127
19. A. Carpentier, et al. Real-time magnetic resonance-guided laser thermal therapy for focal metastatic brain tumors. *Neurosurgery*, 2008, 63(1 Suppl 1): ONS21-8; discussion ONS28-9
20. R. J. Stafford, D. Fuentes, A. A. Elliott, J. S. Weinberg, K. Ahrar. Laser-induced thermal therapy for tumor ablation. *Crit. Rev. Biomed. Eng.*, 2010, 38(1): 79–100
21. C. G. Hadjipanayis, et al. EGFRvIII antibody-conjugated iron oxide nanoparticles for magnetic resonance imaging-guided convection-enhanced delivery and targeted therapy of glioblastoma. *Cancer Res.*, 2010, 70(15): 6303–6312
22. J. H. Sampson, et al., and PRECISE Trial Investigators. Poor drug distribution as a possible explanation for the results of the PRECISE trial. *J. Neurosurg.*, 2010, 113(2): 301–309
23. R. Hamazoe, M. Maeta, N. Kaibara. Intraperitoneal thermochemotherapy for prevention of peritoneal recurrence of gastric cancer. Final results of a randomized controlled study. *Cancer*, 1994, 73(8): 2048–2052
24. Y. Liu, et al. Ultrasound-induced hyperthermia increases cellular uptake and cytotoxicity of P-glycoprotein substrates in multi-drug resistant cells. *Pharm. Res.*, 2001, 18(9): 1255–1261
25. A. H. Saad, G. M. Hahn. Ultrasound-enhanced effects of adriamycin against murine tumors. *Ultrasound Med. Biol.*, 1992, 18(8): 715–723
26. J. B. Block, P. A. Harris, A. Peale. Preliminary observations on temperature-enhanced drug uptake by leukemic leukocytes *in vitro*. *Cancer Chemother. Rep.*, 1975, 59(5): 985–988
27. M. R. DeWitt, A. M. Pekkanen, J. Robertson, C. G. Rylander, M. Nichole Rylander. Influence of hyperthermia on efficacy and uptake of carbon nanohorn-cisplatin conjugates. *J. Biomech. Eng.*, 2014, 136(2): 021003
28. R. L. Hood, R. T. Andriani Jr., S. Emch, J. L. Robertson, C. G. Rylander, J. H. Rossmeisl Jr. Fiberoptic microneedle device facilitates volumetric infusate dispersion during convection-enhanced delivery in the brain. *Lasers Surg. Med.*, 2013, 45(7): 418–426
29. M. A. Kosoglu, R. L. Hood, Y. Chen, Y. Xu, M. N. Rylander, C. G. Rylander. Fiber optic microneedles for transdermal light delivery: *Ex vivo* porcine skin penetration experiments. *J. Biomech. Eng.*, 2010, 132(9): 091014
30. M. A. Kosoglu, et al. Fiberoptic microneedles for microscale interstitial delivery of therapeutic light. *Laser. Surg. Med.*, 2011, 43(9): 914–920
31. R. L. Hood, M. A. Kosoglu, M. Parker, C. G. Rylander. Effects of microneedle design parameters on hydraulic resistance. *J. Med. Device.*, 2011, 5(3): 31012–31016
32. Z. J. Chen, et al. A realistic brain tissue phantom for intraparenchymal infusion studies. *J. Neurosurg.*, 2004, 101(2): 314–322
33. T. Gill, et al. *In vitro* and *in vivo* testing of a novel recessed-step catheter for reflux-free convection-enhanced drug delivery to the brain. *J. Neurosci. Methods*, 2013, 219(1): 1–9
34. R. L. Hood, T. Ecker, R. Andriani, J. Robertson, J. Rossmeisl, C. G. Rylander. Augmenting convection-enhanced delivery through simultaneous co-delivery of fluids and laser energy with a fiberoptic microneedle device. In: I. Gannot, ed. *Proceedings of SPIE 8576: Optical Fibers and Sensors for Medical Diagnostics and Treatment Applications XIII*. San Francisco, CA, USA, 2013
35. F. Casanova, P. R. Carney, M. Sarntinoranont. Influence of needle insertion speed on backflow for convection-enhanced delivery. *J. Biomech. Eng.*, 2012, 134(4): 041006
36. W. Martanto, J. S. Moore, T. Couse, M. R. Prousnitz. Mechanism of fluid infusion during microneedle insertion and retraction. *J. Contrd. Release*, 2006, 112(37): 357–361
37. Z. J. Chen, W. C. Broaddus, R. R. Viswanathan, R. Raghavan, G. T. Gillies. Intraparenchymal drug delivery via positive-pressure infusion: Experimental and modeling studies of poroelasticity in brain phantom gels. *IEEE Trans. Biomed. Eng.*, 2002, 49(2): 85–96
38. Z. J. Chen, W. C. Broaddus, R. R. Viswanathan, R. Raghavan, G. T. Gillies. Intraparenchymal drug delivery via positive-pressure infusion: Experimental and modeling studies of poroelasticity in brain phantom gels. *IEEE Trans. Biomed. Eng.*, 2002, 49(2): 85–96
39. G. T. Gillies, J. H. Smith, J. A. Humphrey, W. C. Broaddus. Positive pressure infusion of therapeutic agents into brain tissues: Mathematical and experimental simulations. *Technol. Health Care*, 2005, 13(4): 235–243
40. S. J. Panse, H. L. Fillmore, Z. J. Chen, G. T. Gillies, W. C. Broaddus. A novel coaxial tube catheter for central nervous system infusions: Performance characteristics in brain phantom gel. *J. Med. Eng. Technol.*, 2010, 34(7-8): 408–414